Enhancing Continuum Robot Mobility: Design and Control with Integrated Dual Rotational DOFs*

Peikang Yuan, Changchao Sun, Xiang Chang, Xu Zhang and Rongjie Kang

***Abstract*— Continuum robots, known for their compliance in unstructured environments, face limitations due to the lack of rotational degrees of freedom (DOFs) about the backbone. This prevents them from compensating undesired torsional deformation and performing 6-DOF control of the end-effector, thereby restricting their mobility. This paper presents a continuum robot with integrated dual rotational DOFs. One is integrated at the arm base to compensate for torsional deformation caused by external loads, while the other one, located at the arm tip, enables full 6-DOF control of the end-effector. To control the robot, a screw-theory-based kinematic model and a kinematic control framework are proposed to enable real-time, simultaneous control of the end-effector's position and orientation. Experimental results show that the arm base rotational joint can fully compensate for undesired torsional deformation caused by a 1000 g payload. Thanks to the arm tip's DOF and the proposed kinematic control framework, the robot's end-effector can maintain a constant orientation while achieving open-loop path-tracking errors of only 3.3% of the arm's length (930 mm), and successfully executing valve-closing tasks with coordinated 6-DOF motion, demonstrating the robot's potential for industrial maintenance, human-robot interaction, and confined-space manipulation.**

I. Introduction

Continuum robots, inspired by the flexible appendages of biological organisms such as elephant trunks and octopus tentacles [1], [2], represent a paradigm shift from traditional rigid-link robots. Unlike their rigid counterparts that rely on discrete joints and links, continuum robots achieve motion through continuous elastic deformation of their body structures, exhibiting theoretically infinite passive degrees of freedom (DOFs) [3], [4]. This unique morphology grants them exceptional compliance and adaptability, making them ideal candidates for applications in unstructured environments. Recent advancements have demonstrated their potential in minimally invasive surgery (MIS) through confined anatomical pathways [5], [6], manipulation in constrained environments [7], [8], and safe physical human-robot (environment) interaction [9], [10].

Despite these advantages, a significant gap remains in their mobility, which is defined as the ability of a mechanical system to achieve independent, controlled motion through its configuration (joint) DOFs [11]. This gap is particularly evident in the challenge of achieving full 6-DOF end-effector control and active torsional compensation under external loads. Most existing systems, whether cable-driven [12], [13], pneumatic-actuated [14], [15], or based on smart materials [16], [17], primarily provided bending and extension DOFs in configuration space through multi-segment arrangements. While these DOFs allow for flexible spatial motion, they inherently lack active rotational control around the continuum arm's backbone. This deficiency in rotational DOFs leads to two primary mobility challenges.

First, undesired torsional deformation caused by external loads or gravitational effects introduces pose error. And it is difficult to compensate the pose error through active control of bending and extending motion. To mitigate the impact of this torsional deformation, current approaches primarily focus on enhancing torsional stiffness without compromising bending and extension capabilities. For instance, Dong proposed a continuum robot consisting of serially connected Twin-Pivot compliant joints [18], which exhibits greater torsional stiffness compared to traditional single-backbone structures. Similarly, Santoso enhanced torsional stiffness using an origami mechanism [19]. While these methods improve torsional stiffness, excessive twisting loads still induce torsional deformation that is hard to be compensated by active control, limiting the performance of continuum robots in high-precision and high-load tasks.

Second, for continuum robots with only bending and extension DOFs, the end-effector typically exhibits 3 translational DOFs (X/Y/Z) and 2 rotational DOFs (pitch/yaw), resulting in a total of 5 DOFs in task space. Notably, advanced control schemes for platforms such as pneumatic-driven [20] and tensegrity-based robots [21] have demonstrated effective pose control for tasks like reaching and pointing. The capabilities of these systems are inherently shaped by their mechanical structure, which relies on bending and extension, and as a result, the axial roll motion is severely restricted [10]. Therefore, while these robots demonstrate effective pose control, our work extends these capabilities. By incorporating full 6-DOF control, our design offers greater mobility in orienting the end-effector. This is particularly crucial for complex manipulations that demand significant axial rotation, such as valve closure and screw assembly,

* This work was supported by the Natural Science Foundation of China (grant no. 52375023, 51975401). (Corresponding author: Rongjie Kang.)

Peikang Yuan, Changchao Sun, Xiang Chang and Xu Zhang are with the Key Laboratory of Mechanism Theory and Equipment Design of Ministry of Education, School of Mechanical Engineering, Tianjin University, Tianjin 300072, China (e-mail: yuanpeikang@tju.edu.cn, sunchangchao@tju.edu.cn, changxiangchina@outlook.com, tju_zhangxu@tju.edu.cn).

Rongjie Kang is with the Key Laboratory of Mechanism Theory and Equipment Design of Ministry of Education, School of Mechanical Engineering, Tianjin University, Tianjin 300072, China (e-mail: rjkang@tju.edu.cn)

thereby broadening the application scope for continuum robots in intricate operational scenarios.

Some studies have incorporated rotational DOFs into continuum robots. For instance, hyper-redundant robots (a type of generalized continuum robot) [22], [23], which were constructed by serially connecting discrete rigid rotational joints, typically use cables to control universal joints, achieving motion akin to continuous bending. These robots generally disregard the effects of torsional deformation while offering a higher load-bearing capacity. However, the rigid joints in such structures result in insufficient compliance and typically lack active rotational DOFs around the arm's axial direction, thereby limiting mobility. To preserve compliance while introducing rotational DOFs, a rigid-flexible coupling structure [24] combines motor-driven rotational joints with continuum modules in series, but introduces additional structural mass.

In this work, we present a continuum robot with integrated dual DOFs to enhance mobility. The first rotational DOF, located at the arm base, primarily enables active compensation for pose error due to torsional deformation. The second rotational DOF, implemented by a cable-driven rotational joint, positioned at the arm tip, allows simultaneous control of all 6 DOFs of the end-effector in most configurations. This integration ensures the arm's compliance while avoiding excessive weight burden. Experimental results demonstrate that this design offers significant advantages, particularly in tasks requiring rotational motion about the axis, such as valve operation.

The rest of the paper is structured as follows: Section II describes the prototype design. Section III presents the kinematic modeling and control framework. In Section IV, a series of experiments were conducted to demonstrate the effectiveness of our design. The conclusions are presented in Section V.

II. Robotic Design

The proposed continuum robot features 2 rotational DOFs and 5 bending DOFs, resulting in a total of 7 DOFs in the configuration space. As shown in Fig. 1(a), the robot's arm base incorporates a hollow rotational joint to accommodate driving cables, sheaths, and communication wires. Rotation is achieved through a servo motor driving a synchronous belt. This joint is connected in series with three independently bending continuum modules, and a cable-driven rotational joint is integrated at the arm tip.

As depicted in Fig. 1(b), Module 1 is a semi-continuum structure, where four offset backbones, made of superelastic NiTi alloy rods, pass through several constraint disks, forming a single-plane spinal structure. This design permits bending exclusively along the normal direction of the spinal plane while providing high bending stiffness in other directions, thereby limiting it to a single bending DOF. To enhance torsional stiffness, a metal bellow (KF16) is integrated at the module's center, with constraint disks rigidly connected to it via a locking mechanism.

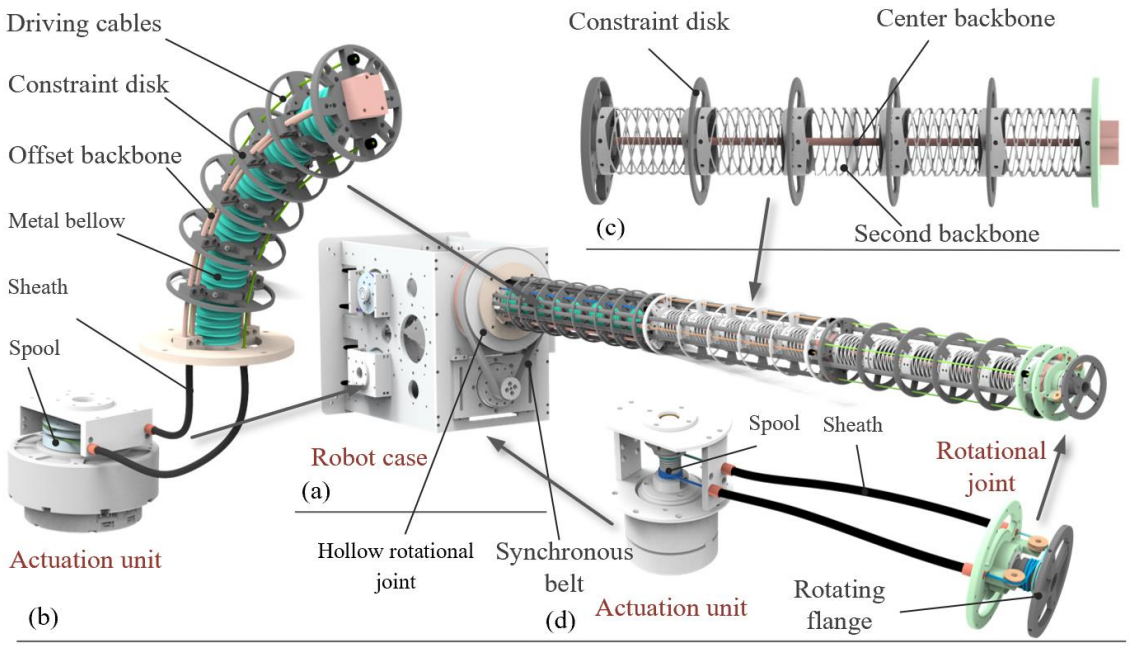

Fig. 1. Prototype Design. (a) Overall structure of the prototype. (b) Structure of Module 1. (c) Structures of Modules 2 and 3. (d) Rotational joint at the arm tip.

To reduce weight, Modules 2 and 3 do not use metal bellows to enhance torsional stiffness. Instead, they adopt a fully-continuum structure with a dual-layer backbone, as shown in Fig. 1(c). Each of these modules has 2 bending DOFs, allowing them to bend in any direction in space. The central backbone consists of super-elastic NiTi alloy rods that primarily provide bending stiffness. The second-layer backbone is composed of several thin-walled hollow metallic cylinders with rhombic grooves, making it compressible and bendable, and these cylinders are rigidly attached to the constraint disks via screws. While this second-layer backbone has lower bending stiffness, it offers superior torsional resistance compared to the central backbone.

A total of 6 actuation units are integrated into the robot case, leaving the entire arm structure free of electronic actuators (motors). 5 of these are used to drive the continuum modules for bending motion, as illustrated in Fig. 1(b). The last actuation unit drives the rotating flange at the arm tip, as shown in Fig. 1(d). Each actuation unit consists of a motor (PDA-14, Produced by Daran Company) driving a spool, which is connected to a pair of driving cables to generate torque. When the spool rotates, one end of the driving cable shortens while the other releases. The cable is covered by a sheath to simplify routing from the spool to the modules and rotating flange.

III. Control

In this Section, the robot's kinematic model will be established first, followed by kinematic control frame based on this model.

A. Kinematic Modeling

As shown in Fig. 2(a), for a continuum module i that can bend in any direction in space, its configuration can be described using 3 parameters: $[\varphi_i \quad \beta_i \quad S_i]$, where φ_i represents the direction angle of the bending plane, β_i represents the bending angle, and S_i is the length of the module i. In our design, the module length S_i is fixed, so the module i has only two adjustable parameters, resulting in 2 DOFs in the configuration space: $q_{c\,i} = [\varphi_i \quad \beta_i]$.

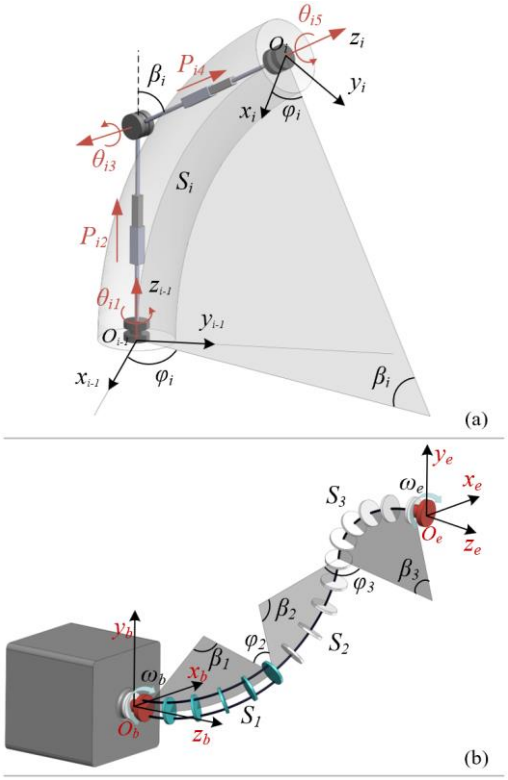

Fig.2. Kinematic model schematic. (a) Kinematic transformation of a single continuum module. (b) Kinematic transformation of the proposed robot.

To establish the transformation relationship from the base coordinate system O_{i-1} to the tip coordinate system O_i for module i, the constant curvature assumption [25] is applied. Based on this assumption, the module i can be modeled as a rigid joint-link mechanism with 3 rotational joint pairs and 2 prismatic joint pairs. The geometric relationships between these 5 joint pairs and the configuration parameters of the module i are as follows:

$$\begin{cases} \theta_{i1} = \varphi_i \\ P_{i2} = S_i \tan(\beta_i / 2) / \beta_i \\ \theta_{i3} = \beta_i \\ P_{i4} = S_i \tan(\beta_i / 2) / \beta_i \\ \theta_{i5} = -\varphi_i \end{cases} \tag{1}$$

The screw coordinates of these 5 joint pairs with respect to the base coordinate system O_{i-1} can be expressed as:

$$\begin{cases} \xi_{i1} = [0 \quad 0 \quad 1 \quad 0 \quad 0 \quad 0]^T \\ \xi_{i2} = [0 \quad 0 \quad 0 \quad 0 \quad 0 \quad 1]^T \\ \xi_{i3} = [0 \quad -1 \quad 0 \quad 0 \quad 0 \quad 0]^T \\ \xi_{i4} = [0 \quad 0 \quad 0 \quad 0 \quad 0 \quad 1]^T \\ \xi_{i5} = [0 \quad 0 \quad -1 \quad 0 \quad 0 \quad 0]^T \end{cases} \tag{2}$$

The kinematic transformation of module i can then be expressed as an Product of Exponentials (PoE) formula [26], i.e.,

$$T^i_{\text{sec}}(\varphi_i, \beta_i) = e^{\zeta_{i1}\theta_{i1}} e^{\zeta_{i2}P_{i2}} e^{\zeta_{i3}\theta_{i3}} e^{\zeta_{i4}P_{i4}} e^{\zeta_{i5}\theta_{i5}} T^i_{\text{sec}}(\varphi_i = 0, \beta_i = 0) \tag{3}$$

For the robot we have designed, which includes 2 rotational joints and 3 continuum modules, a total of 7 DOFs exist in its configuration space, as shown in Fig. 2(b):

$$q_c = [\omega_b \quad \beta_1 \quad \varphi_2 \quad \beta_2 \quad \varphi_3 \quad \beta_3 \quad \omega_e] \tag{4}$$

Here, ω_b and ω_e denote the angles of the rotational joints at the base and the tip of the arm, respectively. β_i and φ_i represent the bending angle and direction angle of module i (i=1,2,3), respectively. Since module 1 has only a single bending DOF, it lacks a direction angle. The screw coordinates of both rotational joints with respect to the base coordinate system O_b are:

$$\xi_{R\_1} = \xi_{R\_2} = [0 \quad 0 \quad 1 \quad 0 \quad 0 \quad 0]^T \tag{5}$$

Thus, the PoE formula for these two rotational joints are:

$$\begin{cases} T^1_{rot}(\omega_b) = e^{\zeta_{R\_1}\omega_b} T^1_{rot}(\omega_b = 0) \\ T^2_{rot}(\omega_e) = e^{\zeta_{R\_2}\omega_e} T^2_{rot}(\omega_e = 0) \end{cases} \tag{6}$$

The PoE formula for each continuum module is given in Equation (3). Since Module 1 lacks a direction angle, its PoE simplifies to:

$$T^1_{\text{sec}tion}(\beta_1) = e^{\zeta_{12}P_{12}} e^{\zeta_{13}\theta_{13}} e^{\zeta_{14}P_{14}} T^1_{\text{sec}tion}(\beta_1 = 0) \tag{7}$$

Based on the transformation relationships of these joints and modules, the robot's forward kinematics can be expressed as:

$$T_{\text{robot}} = T^1_{\text{rot}}(\omega_b) T^1_{\text{sec}}(\beta_1) T^2_{\text{sec}}(\varphi_2, \beta_2) T^3_{\text{sec}}(\varphi_3, \beta_3) T^2_{\text{rot}}(\omega_e) M \tag{8}$$

Here, $M \in SE(3)$ denotes the pose matrix of the end-effector when the robot is in its initial configuration, where all

configuration parameters are zero and the arm is in a straight state.

B. Kinematic Control Framework

In robotic applications, the position and orientation of the robot's end-effector typically need to be controlled simultaneously to perform various tasks. The forward kinematic model T_{robot}, derived in Equation (8), can also be represented as the end-effector's pose matrix, i.e.,

$$T_e = T_{robot} = \begin{bmatrix} R_e & P_e \\ 0 & 1 \end{bmatrix} \tag{9}$$

Here, the rotation matrix $R_e \in SO(3)$ defines the orientation of the end-effector with respect to the base coordinate system O_b , while the three-dimensional vector P specifies its position relative to O_b .

As shown in Fig. 3, to control the position and orientation of the robot's end-effector, translation or rotation commands can be generated. The target pose matrix of the end-effector, T_{target} , is then obtained:

$$T_{\text{target}} = \begin{cases} T_{robot} Trans(x_{step}, y_{step}, z_{step}) \\ T_{robot} Rot(X/Y/Z, \theta_{step}) \end{cases} \tag{10}$$

Here, $Trans(x_{step}, y_{step}, z_{step})$ denotes the translation command (operator), representing the translation matrix along the XYZ directions, where x_{step}, y_{step}, z_{step} are the corresponding translation steps. $Rot(X/Y/Z, \theta_{step})$ denotes the rotation command (operator), representing the rotation matrix around the X, Y, or Z axis, with θ_{step} as the rotation step. By right-multiplying these transformation commands (operators), the end-effector's pose matrix T_{robot} is updated to obtain the target pose matrix T_{target} .

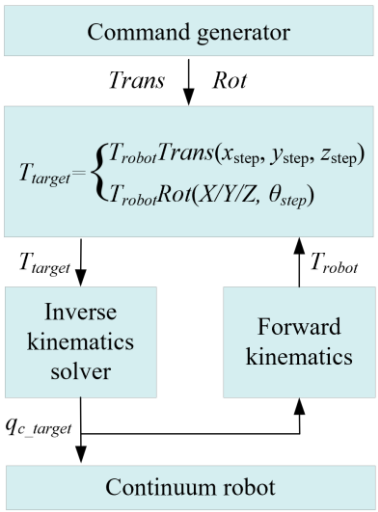

Fig. 3. Schematic of the robotic kinematic control framework.

After obtaining the target pose matrix T_{target}, the inverse kinematics solver computes the corresponding target configuration q_{c_target}. In this paper, the inverse kinematics solver is a numerical solver based on the Newton-Raphson iterative metho [27]. Once q_{c_target} is determined, the continuum robot is controlled to reach this target configuration q_{c_target}. Simultaneously, the forward kinematic model updates the end-effector's pose matrix T_{robot}, preparing for the next motion command.

IV. Experiment And Demonstration

This section first tests how the proposed continuum robot compensates for undesired torsional deformation using the rotational DOF at the arm base. It then evaluates motion accuracy through a path-tracking experiment, utilizing both the rotational DOF at the arm tip and the kinematic control framework, followed by a demonstration of valve closure to showcase the overall mobility of the proposed robot.

A. Torsional Deformation Compensation Experiment

This experiment aims to demonstrate that the proposed continuum robot can compensate undesired torsional deformation through the rotational joint at its arm base. As shown in Fig. 4(a), the robot is placed horizontally, and the 3 continuum modules are bent 30° each in the same direction, forming a semi-C-shaped configuration with an overall bend of 90°. A 1000 g payload is placed at the arm tip, introducing a torsional torque at the arm base. Although the designed continuum arm has been structurally enhanced to improve torsional stiffness (by introducing metal bellows and a dual-layer backbone structure, as described in Section 2), significant torsional deformation still occurs under this payload. However, by rotating the base's rotational joint by 31.5° in the opposite direction of the load-induced torque, the arm tip can be returned to its position prior to the load-induced deformation. This demonstrates that the undesired torsional deformation can be fully compensated, as shown in Fig. 4(b). This experiment demonstrates that the integrated rotational DOF at the base enables the continuum robot to actively compensate for undesired torsional deformation, thereby improving its mobility in configuration space.

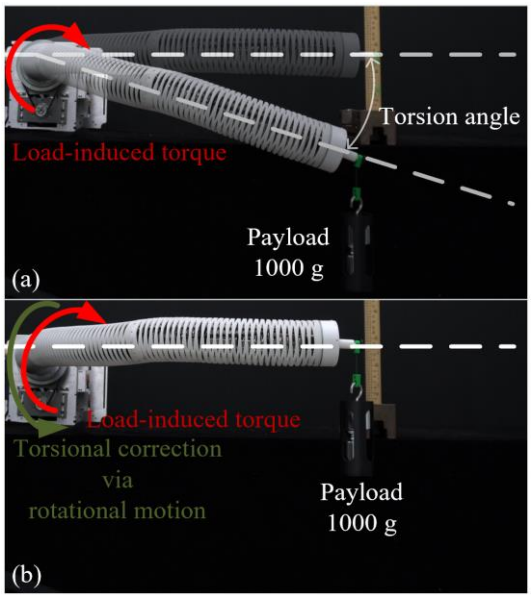

Fig. 4. Torsional deformation compensation experiment. (a) Before compensation. (b) Compensation via the base rotational joint.

B. Path Tracking Experiment

To test the robot's mobility and its motion accuracy in task space, we conducted a path tracking experiment based on the

kinematic control framework proposed in Section III-B. As shown in Fig. 5, we used the proposed kinematic control framework to have the robot track two paths: a rectangular path measuring 300×200 mm and a circular path with a diameter of 300 mm. Optical markers were attached to the arm tip, and a NOKOV motion capture system (Mars1.3H, 3D positioning accuracy ±0.2 mm) was used to record the actual path.

The experimental results show that the maximum error for the rectangular path tracking was 30 mm, while the maximum error for the circular path tracking was 20 mm. The error arises from the kinematic modeling based on constant curvature, which inherently introduces modeling inaccuracies. Additionally, the measurements were taken under open-loop control. Notably, the maximum error (30 mm) represents only 3.3% of the arm length (930 mm). Based on our previous research [28], incorporating closed-loop correction methods such as visual servoing, the robot's final positioning accuracy can reach ±1 mm under this initial open-loop positioning accuracy.

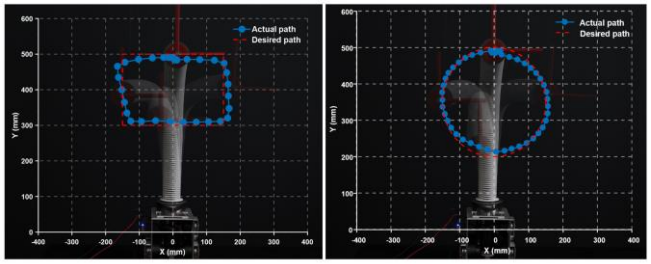

(a) (b)

Fig. 5. Path-tracking experiment. (a) Rectangular path, (b) Circular path.

Overall, the tracking performance for the circular path was better than for the rectangular path, likely due to the sharp direction changes at the corners of the rectangular path, which made it more difficult to track. Notably, during the entire path tracking experiment, we maintained a constant orientation for the robot's end effector. This indicates that we can control all 6 DOFs of the robot's end effector for Cartesian motion in task space. This capability is enabled by the integration of a rotational DOF at the robot's arm tip. The complete experimental procedure is available in Supplementary Video Material's part 1. The results demonstrate that the designed continuum robot is capable of performing complex operations with its end effector.

C. Valve Closing Demonstration

As discussed earlier, the integration of rotational DOFs in continuum robots enhances their mobility. In particular, the rotational DOF at the end-effector is highly suited for tasks requiring rotational motion, such as valve closing. As shown in Fig. 6, a two-finger gripper is integrated at the arm tip as end-effector, which is used to close a valve and stop gas leakage. Steps 1 to 4 in Fig. 6 illustrate the complete valve closing process. From Step 1 to Step 2, the robot moves from its initial configuration to a pre-determined one that aligns with the valve. From Step 2 to Step 3, the proposed kinematic control framework is used to guide the robot to move along the axis of the end-effector to grip the valve.

Finally, in Step 4, a rotational command is applied to rotate the end-effector, closing the valve and halting the gas leakage. A demonstration video is available in Supplementary Video Material's part 2. This demonstration highlights the proposed continuum robot's exceptional mobility and its capability to perform complex tasks.

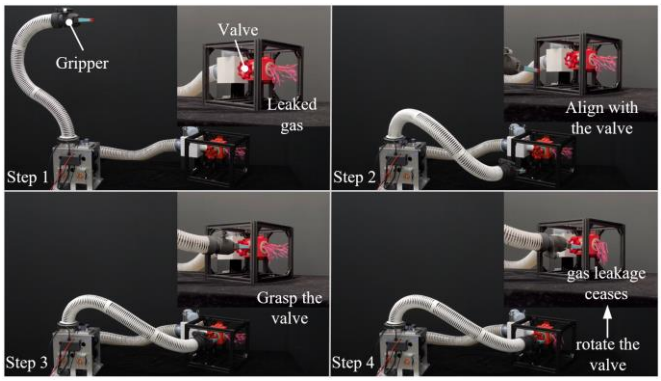

Fig. 6. Valve Closing Demonstration

V. Conclusion

This paper proposed a continuum robot design that integrates two rotational DOFs, enhancing the mobility of the continuum robot. The design addressed the challenges of undesired torsional deformation and limited end-effector DOFs in conventional continuum robots.

In our robot, two rotational DOFs were integrated into the continuum robot: one at the arm base for torsional compensation and another at the arm tip for 6-DOF control of the end-effector (position and orientation). A screw-theory-based kinematic model and kinematic control framework enable accurate path tracking, demonstrated by path-following experiments with errors below 3.3% of the arm length. The valve-closing demonstration highlights the robot's mobility in performing complex tasks that require synchronized translation and rotation of the end-effector.

Future work will focus on enhancing the robot's interaction capability by introducing interactive force control, enabling better application in unstructured environments. This research advances continuum robotics and broadens their practical applications in real-world scenarios.

Acknowledgment

This work was supported by the Natural Science Foundation of China (grant no. 52375023, 51975401).

References

[1] J. Zhang *et al.*, "A Preprogrammable Continuum Robot Inspired by Elephant Trunk for Dexterous Manipulation," *Soft Robot.*, vol. 10, no. 3, pp. 636–646, Jun. 2023, doi: 10.1089/soro.2022.0048.

[2] S. Kolachalama and S. Lakshmanan, "Continuum Robots for Manipulation Applications: A Survey," *J. Robot.*, vol. 2020, no. 1, p. 4187048, 2020, doi: 10.1155/2020/4187048.

[3] M. Russo *et al.*, "Continuum Robots: An Overview," *Adv. Intell. Syst.*, vol. 5, no. 5, p. 2200367, 2023, doi: 10.1002/aisy.202200367.

[4] C. Yang, I. D. Walker, D. T. Branson, J. S. Dai, T. Sun, and R. Kang, "A Multitentacle Gripper for Dynamic Capture," *IEEE Trans. Robot.*, vol. 40, pp. 4284–4300, 2024, doi: 10.1109/TRO.2024.3454437.

[5] P. E. Dupont, N. Simaan, H. Choset, and C. Rucker, "Continuum Robots for Medical Interventions," *Proc. IEEE*, vol. 110, no. 7, pp. 847–870, Jul. 2022, doi: 10.1109/JPROC.2022.3141338.

[6] C. Shi *et al.*, "Shape Sensing Techniques for Continuum Robots in Minimally Invasive Surgery: A Survey," *IEEE Trans. Biomed. Eng.*, vol. 64, no. 8, pp. 1665–1678, Aug. 2017, doi: 10.1109/TBME.2016.2622361.

[7] P. Yuan *et al.*, "Design of a Deployable Continuum Robot (DCR) With Coiling Mechanism," *IEEEASME Trans. Mechatron.*, pp. 1–13, 2025, doi: 10.1109/TMECH.2025.3572012.

[8] X. Dong *et al.*, "Continuum Robots Collaborate for Safe Manipulation of High-Temperature Flame to Enable Repairs in Challenging Environments," *IEEEASME Trans. Mechatron.*, vol. 27, no. 5, pp. 4217–4220, Oct. 2022, doi: 10.1109/TMECH.2021.3138222.

[9] C. Abah, A. L. Orekhov, G. L. H. Johnston, and N. Simaan, "A Multi-Modal Sensor Array for Human–Robot Interaction and Confined Spaces Exploration Using Continuum Robots," *IEEE Sens. J.*, vol. 22, no. 4, pp. 3585–3594, Feb. 2022, doi: 10.1109/JSEN.2021.3140002.

[10] H. Jiang *et al.*, "Hierarchical control of soft manipulators towards unstructured interactions," *Int. J. Robot. Res.*, vol. 40, no. 1, pp. 411–434, Jan. 2021, doi: 10.1177/0278364920979367.

[11] J. S. Dai, D. Li, Q. Zhang, and G. Jin, "Mobility analysis of a complex structured ball based on mechanism decomposition and equivalent screw system analysis," *Mech. Mach. Theory*, vol. 39, no. 4, pp. 445–458, Apr. 2004, doi: 10.1016/j.mechmachtheory.2003.12.004.

[12] T.-D. Nguyen and J. Burgner-Kahrs, "A tendon-driven continuum robot with extensible sections," in *2015 IEEE/RSJ International Conference on Intelligent Robots and Systems (IROS)*, Sep. 2015, pp. 2130–2135. doi: 10.1109/IROS.2015.7353661.

[13] Z. Yang, L. Yang, Y. Sun, and X. Chen, "Comprehensive kinetostatic modeling and morphology characterization of cable-driven continuum robots for in-situ aero-engine maintenance," *Front. Mech. Eng.*, vol. 18, no. 3, p. 40, Oct. 2023, doi: 10.1007/s11465-023-0756-0.

[14] Z. Li, H. Chen, F. Xu, and H. Wang, "An Origami-Inspired Pneumatic Continuum Module with Active Variable Stiffness," in *2024 IEEE/RSJ International Conference on Intelligent Robots and Systems (IROS)*, Oct. 2024, pp. 8293–8298. doi: 10.1109/IROS58592.2024.10801420.

[15] R. Kang, Y. Guo, L. Chen, D. T. Branson, and J. S. Dai, "Design of a Pneumatic Muscle Based Continuum Robot With Embedded Tendons," *IEEEASME Trans. Mechatron.*, vol. 22, no. 2, pp. 751–761, Apr. 2017, doi: 10.1109/TMECH.2016.2636199.

[16] J. Zhang *et al.*, "Bioinspired Continuum Robots with Programmable Stiffness by Harnessing Phase Change Materials," *Adv. Mater. Technol.*, vol. 8, no. 6, p. 2201616, 2023, doi: 10.1002/admt.202201616.

[17] Y. Kim and J. P. Desai, "Design and kinematic analysis of a neurosurgical spring-based continuum robot using SMA spring actuators," in *2015 IEEE/RSJ International Conference on Intelligent Robots and Systems (IROS)*, Sep. 2015, pp. 1428–1433. doi: 10.1109/IROS.2015.7353555.

[18] X. Dong, M. Raffles, S. Cobos-Guzman, D. Axinte, and J. Kell, "A Novel Continuum Robot Using Twin-Pivot Compliant Joints: Design, Modeling, and Validation," *J. Mech. Robot.*, vol. 8, no. 021010, Nov. 2015, doi: 10.1115/1.4031340.

[19] J. Santoso and C. D. Onal, "An Origami Continuum Robot Capable of Precise Motion Through Torsionally Stiff Body and Smooth Inverse Kinematics," *Soft Robot.*, vol. 8, no. 4, pp. 371–386, Aug. 2021, doi: 10.1089/soro.2020.0026.

[20] J. Shi, S.-A. Abad, J. S. Dai, and H. A. Wurdemann, "Position and Orientation Control for Hyperelastic Multisegment Continuum Robots," *IEEEASME Trans. Mechatron.*, vol. 29, no. 2, pp. 995–1006, Apr. 2024, doi: 10.1109/TMECH.2023.3338955.

[21] F. Li, H. Yang, G. Gu, Y. Wang, and H. Peng, "Position and Orientation Tracking Control of a Cable-Driven Tensegrity Continuum Robot," *IEEE Trans. Robot.*, vol. 41, pp. 1791–1811, 2025, doi: 10.1109/TRO.2025.3543292.

[22] J. Peng, W. Xu, T. Yang, Z. Hu, and B. Liang, "Dynamic modeling and trajectory tracking control method of segmented linkage cable-driven hyper-redundant robot," *Nonlinear Dyn.*, vol. 101, no. 1, pp. 233–253, Jul. 2020, doi: 10.1007/s11071-020-05764-7.

[23] W. Xu, T. Liu, and Y. Li, "Kinematics, Dynamics, and Control of a Cable-Driven Hyper-Redundant Manipulator," *IEEEASME Trans. Mechatron.*, vol. 23, no. 4, pp. 1693–1704, Aug. 2018, doi: 10.1109/TMECH.2018.2842141.

[24] X. Jing, J. Jiang, F. Xie, C. Zhang, S. Chen, and L. Yang, "Continuum Manipulator With Rigid-Flexible Coupling Structure," *IEEE Robot. Autom. Lett.*, vol. 7, no. 4, pp. 11386–11393, Oct. 2022, doi: 10.1109/LRA.2022.3199683.

[25] R. J. WebsterIII and B. A. Jones, "Design and Kinematic Modeling of Constant Curvature Continuum Robots: A Review," *Int. J. Robot. Res.*, vol. 29, no. 13, pp. 1661–1683, Nov. 2010, doi: 10.1177/0278364910368147.

[26] C. Yang, R. Kang, D. T. Branson, L. Chen, and J. S. Dai, "Kinematics and statics of eccentric soft bending actuators with external payloads," *Mech. Mach. Theory*, vol. 139, pp. 526–541, Sep. 2019, doi: 10.1016/j.mechmachtheory.2019.05.015.

[27] A. Goldenberg, B. Benhabib, and R. Fenton, "A complete generalized solution to the inverse kinematics of robots," *IEEE J. Robot. Autom.*, vol. 1, no. 1, pp. 14–20, Mar. 1985, doi: 10.1109/JRA.1985.1086995.

[28] L. Chang *et al.*, "Visual-Servo Based End-Effector Control for Continuum Robots," in *2023 International Conference on Advanced Robotics and Mechatronics (ICARM)*, Jul. 2023, pp. 380–385. doi: 10.1109/ICARM58088.2023.10218886.